



Application of an artificial neural network–genetic algorithm methodology for modelling and optimization of the improved biosorption of a chemically modified peat moss: kinetic studies

Clint Sutherland^{a,*}, Beverly S. Chittoo^a, Chintanapalli Venkobachar^b

^a*Project Management and Civil Infrastructure Systems, The University of Trinidad and Tobago, San Fernando Campus, Trinidad and Tobago (WI), Tel. +1 868 497 5744; email: clint.sutherland@utt.edu.tt (C. Sutherland), Tel. +1 868 491 6879; email: beverly.chittoo@utt.edu.tt (B.S. Chittoo)*

^b*Department of Civil and Environmental Engineering (Retired), The University of the West Indies, St. Augustine, Trinidad and Tobago (WI), email: cvenkobachar@gmail.com*

Received 27 March 2017; Accepted 9 July 2017

ABSTRACT

In this study, peat moss was chemically modified using a hot-alkali treatment technique and subsequently used to remove Cu(II) and Pb(II) ions from synthetic solutions. Batch kinetic studies were carried out to elucidate the mechanisms of biosorption. Process operational parameters such as agitation, particle size, conductivity and pH were varied. This method of hot-alkali treatment was successful in reducing the occlusion of pores and resulted in greater adsorptive performance. The kinetic behaviour of the treated peat moss was best simulated by the diffusion–chemisorption model. Film diffusion and intraparticle diffusion were the dominant transport mechanisms. An artificial neural network (ANN) was used to construct a predictive model built-in with the joint effect of the operating parameters. A comparison with the experimental data revealed a significantly high coefficient of determination of 0.9965. The Garson connection weight method showed reaction time as the most influential parameter. Artificial neural network–genetic algorithm (ANN–GA) optimization revealed that maximum biosorption could be obtained using pH 5.5, particle size 0.21 mm, agitation 690 rpm, conductivity 290 $\mu\text{S}/\text{cm}$ and contact time 50 min. The ANN–GA prediction was verified through subsequent laboratory experiments which revealed an excellent prediction with 2.8% residual error. The findings of this study serve to improve the performance of peat biosorption as well as presents a predictive model which can aid in process scale-up.

Keywords: Biosorption; Kinetics; Heavy metal; Peat moss; Artificial neural network; Genetic algorithm

1. Introduction

There have been numerous reported episodes of acute and chronic impacts on human health caused by heavy metal contamination [1,2]. These reports and others have been confirmed through current advances in metal detection at the nanolevel and have led to increased stringent controls being imposed on those industries responsible for the discharge of toxic metals in their effluents [3]. As a result,

improved technologies are being sought to achieve the low effluent metal concentrations demanded by new legislations; unfortunately, the greatest impact would be felt by smaller downstream industries that are unable to sustain exorbitant treatment costs [4]. The ultimate solution lies in low-cost technologies enabling both removal and recovery of heavy metals [5]. Consequently, these needs provide sufficient interest to undertake this study.

The most common technique for recovery of metal ions from industrial waste is by precipitation, either as hydroxide, carbonate or sulphide. However, there are disadvantages to this method mostly due to unsatisfactory treatment

* Corresponding author.

levels at low metal concentrations [6]. Ion-exchange is also a well-established process used in tertiary treatment; however, the cost of resin and regenerating chemicals renders this technique less than ideal [7].

Early researchers in the field of biosorption as McKay et al. [8], Tsezos and Volesky [9], and Bhattacharya and Venkobachar [10], have shown biological materials to be very effective in removing metal ions from solutions, achieving low residual metal concentrations and high metal loading. Additionally, many low-cost adsorbents come from the abundant biological materials found in nature such as unicellular algae [11], plant leaves [12], macro-fungus [13] and bacteria [14]. In a review of biosorption technologies and applications, Gadd [15], highlighted that future biosorption research direction should include identification of better and more selective biosorbents, more development of biosorption models and identification of biosorption mechanisms.

To elucidate the mechanisms of biosorption, an understanding of how metal ions are transferred from a liquid phase to a solid phase is essential. According to Poots et al. [16], the following steps are usually involved: (i) boundary layer mass transfer across the liquid film surrounding the particle; (ii) internal diffusion/mass transport within the particle boundary as pore and/or solid diffusion and (iii) adsorption within the particle and on the external surface. Allard et al. [17] explained that there are three pathways by which sorption may occur onto the surface: (i) physical adsorption which is considered rapid and reversible and is due to non-specific forces of attraction (e.g., Van der Waals forces); (ii) electrostatic adsorption due to coulombic forces of attraction between charged solute species and the adsorbing phase – this process is usually rapid and largely reversible; and (iii) specific adsorption due to the action of chemical forces of attraction which leads to surface bonding at a specific site on the solid phase.

Peat moss has been reported to comprise a rich array of polar functional groups such as alcohol, aldehydes, carboxylic acids, ketones and phenolic hydroxides which are suitable for sorption or ion-exchange processes [18]. Due to the abundance, there have been numerous reported techniques of peat moss pretreatment, all aimed at improving its biosorption performance. Some of these techniques include acid followed by cold-alkali treatment [19], pyrolysis [20] and hot-acid followed by cold-alkali treatment [21]. All of which have proven to be successful depending on the target contaminant. However, the application of hot-alkali treatment [13], to peat moss has not been reported in the literature. The performance of this modified peat is assessed by studying sorption kinetics. Such studies evaluate the rate of metal uptake and provide a deeper understanding of the reaction pathways and mechanisms [22].

The development of predictive models can save time and improve efficiency in experimentation and enable the effectual upgrade to full-scale systems [23]. Due to the non-linearity and diversity of biosorption systems, it is difficult to develop predictive models based on traditional single variable optimization [24]. Kumar and Sharma [25] explained in their review of artificial neural networks (ANNs) that these intelligent systems are inspired by the neural structure of the human brain. The first artificial neuron was produced in 1943 by McCulloch and Pitts [26]. The technique has seen application in gaming development, pattern recognition and complex engineering processes [27]. An ANN based on the common multilayer

perceptron consist of input, output and hidden layers of neurons and is a powerful tool for modelling of data [28]. Shahryari et al. [29] explained that the number of neurons in the input and output layers are the same as the number of the known independent and dependent parameters, respectively. The successful application of ANN to predict complex biosorption processes have been reported in the literature. Cojocaru et al. [30] developed an ANN to predict the removal efficiency of oil slick by peat moss and used biosorbent dosage, drainage time and initial thickness of the oil slick as inputs to predict the removal efficiency. Chowdhury et al. [31] predicted the sorption of crystal violet dye onto eggshells by constructing an ANN with pH, biosorbent dose, initial dye concentration and temperature as inputs to the ANN while sorption efficiency was selected as the output. In this study, batch biosorption kinetic operational parameters such as agitation speed, pH, reaction time, conductivity and biosorbent size (independent variables) were instituted as input to the ANN structure to predict biosorption removal (dependent variable). A genetic algorithm (GA) is a stochastic search algorithm inspired by the mechanics of natural evolution including survival of the fittest, reproduction, crossover and mutation [32]. The robustness of this global optimization method has also gained widespread acceptance in the field of engineering [33]. The generation of global optimal operating adsorption parameters has been successfully attained by the use of GA coupled with output from the ANN (ANN-GA) [34,35].

The objectives of this study are: (i) to evaluate the impact and performance of this method of hot-alkali pretreatment to peat moss and expound its mechanisms of biosorption through kinetic study and analysis; (ii) to develop a predictive model based on ANN to simulate batch process kinetics which can aid in process scale-up; and (iii) to optimize the amount of heavy metals removed from solution by combining ANN and GA methods.

2. Materials and methods

2.1. Preparation of the biosorbent

Batch biosorption experiments were conducted with Canadian sphagnum peat moss manufactured by Acadian Limited, Canada. In preparation for biosorption experiments, the peat samples were dried at 90°C for 1 h. It was subsequently washed with distilled water and sieved into different sizes. The average particle size of peat moss retained on a sieve was calculated as the geometric mean of the diameter openings in two adjacent sieves in the stack. The geometric mean size (GMS) is expressed as $(\text{diameter of upper sieve} \times \text{diameter of lower sieve})^{0.5}$ [36]. Kinetic experiments were conducted using particle GMS of 0.11–1.05 mm. Peat moss samples were chemically treated using the hot-alkali pretreatment procedure previously reported by Muraleedharan and Venkobachar [13]. 40 g of the biosorbent was treated with 100 mL of 40% NaOH at 128°C for 4 h. The residue was then separated, washed with distilled water and dried at 40°C for 24 h.

2.2. Determination of metal ions concentration

Metal ions selected for these experiments were Cu(II) and Pb(II) ions and were analyzed using an Atomic Absorption

Spectrophotometer (PerkinElmer 3030B). Analytical grade copper(II) sulphate and lead(II) nitrate were used to prepare stock solutions in distilled water (using a Corning Mega Pure System MP-1 of pH ~7 and conductivity <5 $\mu\text{S}/\text{cm}$).

2.3. Scanning electron microscopy combined with energy-dispersive spectroscopy analysis

The biosorbent was characterized using a scanning electronic microscope (SEM; Hitachi S-3000N) and energy-dispersive spectroscopy (EDS) analyzer (IXRF Systems) at a voltage of 20 kV. The SEM was used to investigate the changes in the surface microstructures of the peat before and after pretreatment as well as following metal ion biosorption. The EDS was used to determine the elemental composition of the peat before pretreatment, after pretreatment and after metal ion biosorption.

2.4. Biosorption kinetics

2.4.1. Kinetic studies

Kinetic studies were conducted using the parallel method according to EPA OPPTS method 835.1230 [37]. The studies of metal uptake were carried out in duplicate at room temperature ($26^\circ\text{C} \pm 2^\circ\text{C}$) in a batch reactor with an adsorbent mass 1.0 g/L and spiked with 50 mL of 50 mg/L synthetic metal ion solution. Sorbent masses were accurate to ± 0.001 g and solution volumes to ± 0.5 mL. Identical reaction mixtures were prepared for each time interval, agitated to maintain complete mixed conditions on a mechanical shaker and removed at predetermined time intervals [38]. The biosorbent was then separated by filtration using Whatman No. 2 qualitative filter paper. The filtrate/supernatant was subsequently tested for residual metal ions. To monitor and control any interference due to leaching during the test period a blank was prepared which comprised distilled water and peat moss. Optimum pH was determined by adjusting the pH within the range of 2.5–6 and kept constant throughout the reaction by a 0.01 M acetate buffer solution and measured with a pH meter (Accumet Research-AR10, Fisher Scientific, New Hampshire, USA). The conductivity of the reaction solution was adjusted using potassium nitrate solution and measured using a conductance bridge (YSI Model 31A).

2.4.2. Adsorption yield

The adsorption yield or the ratio of adsorbed metal ion concentration to the initial metal ion concentration was calculated from Eq. (1):

$$\% \text{ Adsorption} = \frac{C_0 - C_t}{C_0} \times 100 \quad (1)$$

where C_0 (mg/L) is the initial concentration of metal ions in solution, C_t (mg/L) is the concentration of metal ions in solution at any time t .

2.4.3. Concentration of adsorbed ions

The concentration of metal ions on peat moss was determined using the mass balance equation expressed as follows:

$$q_t = \frac{(C_0 - C_t)}{m} \times V \quad (2)$$

where q_t (mg/g) is milligram of adsorbate adsorbed per gram of sorbent at any time t , C_0 (mg/L) is the initial adsorbate concentration in solution, C_t (mg/L) is the adsorbate concentration in solution at any time t , V (L) is the volume of synthetic adsorbate solution and m (g) is the mass of the adsorbent.

2.5. Modelling and optimization approach

2.5.1. Kinetic models

2.5.1.1. Lagergren model In 1898, Lagergren as cited in [39], developed a first-order rate equation to describe the kinetic process of oxalic acid and malonic acid onto charcoal. Ho and McKay [39] described the equation as pseudo-first-order. Table 1 presents the non-linear and linear forms of the pseudo-first-order model represented by Eqs. (3) and (4), respectively, where K_{PFO} (min^{-1}) is the rate constant of pseudo-first-order adsorption, q_t (mg/g) is the mass of adsorbate sorbed per gram of adsorbent at any time t (min) and q_e (mg/g) is the mass of adsorbate sorbed per gram of adsorbent at equilibrium.

Table 1
Linear and non-linear kinetic models

Model	Non-linear equation	Eq.	Linear equation	Eq.
Pseudo-first-order model	$q_t = q_e(1 - \exp^{-K_{\text{PFO}}t})$	(3)	$\log(q_e - q_t) = \log q_e - \frac{K_{\text{PFO}}}{2.303}t$	(4)
Pseudo-second-order model	$q_t = \frac{K_{\text{PSO}}q_e^2t}{1 + K_2q_e t}$	(5)	$\frac{t}{q_t} = \frac{1}{K_{\text{PSO}}q_e^2} + \frac{t}{q_e}$	(6)
Intraparticle diffusion model	$q_t = K_{\text{id}}(t^{1/2})$	(7)	$q_t = K_{\text{id}}(t^{1/2}) + c$	(8)
Diffusion–chemisorption model	$q_t = \frac{1}{\frac{1}{q_e} + \frac{t^{0.5-1}}{K_{\text{DC}}}}$	(9)	$\frac{t^{0.5}}{q_t} = \frac{t^{0.5}}{q_e} + \frac{1}{K_{\text{DC}}}$	(10)

2.5.1.2. Pseudo-second-order model The pseudo-second-order equation was developed for the sorption of divalent metal ions onto peat moss [40]. According to Ho and McKay [41], the model is based on pseudo-second-order chemical reaction kinetics. Linear and non-linear forms of the model are presented in Table 1, where K_{psO} (g/mg min) is the pseudo-second-order rate, q_t (mg/g) is the mass of adsorbate adsorbed per gram of adsorbent at any time t (min), q_e (mg/g) is the mass of adsorbate adsorbed per gram of adsorbent at equilibrium and h (mg/g t) is the initial rate of adsorption given by $K_{\text{psO}} \times q_e^2$.

2.5.1.3. Intraparticle diffusion model Weber and Morris [42] proposed that the rate of intraparticle diffusion varies proportionally with the half power of time and is expressed as Eq. (7). According to Ofomaja [43], the model can be linearized to Eq. (8) where q_t (mg/g) is the adsorbate uptake at time t (min), K_{id} (mg/g t^{0.5}) is the rate constant of intraparticle transport and the intercept c (mg/g), is taken to be proportional to the extent of the boundary layer thickness. According to Weber and Morris [42], if the rate-limiting step is intraparticle diffusion, a plot of solute adsorbed against the square root of the contact time should yield a straight line passing through the origin.

2.5.1.4. Diffusion–chemisorption model The diffusion–chemisorption kinetic model [44] was developed to simulate sorption of heavy metals onto heterogeneous media. To obtain the derivatives, a correlation is made where the rate of change of concentration of the solid phase q_t (mg/g) is equated as a function of the rate of mass transfer of ions from the fluid phase to the adsorption site K_{DC} (mg/g t^{0.5}); the equilibrium sorption capacity q_e (mg/g); and time to the power of $n - 1$, t^{n-1} . Linear and non-linear forms of the model are presented in Table 1, where K_{DC} (g/mg min) is the diffusion–chemisorption constant, q_t (mg/g) is the mass of ions adsorbed per gram of sorbent at any time t (min), q_e (mg/g) is the adsorption at equilibrium and k_i (mg/g t) is the initial adsorption rate given by K_{DC}^2/q_e .

2.5.1.5. External mass transfer model The model expresses the concentration of the solute in the solution as a function of the difference in concentration of the solute in the solution, C , and at the particle surface, C_f according to the following equation [45]:

$$\frac{dq}{dt} = -k_f S_0 (C - C_i) \quad (11)$$

Since C_i approaches zero and C approaches C_0 as $t \rightarrow 0$, Eq. (11) could be simplified to:

$$\left[\frac{d(C/C_0)}{dt} \right]_{t=0} = -k_f S_0 \quad (12)$$

where q (mg/g) is the average solute concentration in the solid, C (mg/L) is the uniform concentration of the solute in the bulk of the liquid, far from the surface, C_i (mg/L) is

the concentration of the solute in the liquid at the particle/liquid interface and k_f (cm/min) is the film mass transfer coefficient. Assuming the particles are spherical, the surface area for mass transfer, S_0 (cm²) can be obtained from the following [46]:

$$S_0 = \frac{6m_s}{d_p \rho (1 - \epsilon_p)} \quad (13)$$

where m_s (g/cm³) is the mass of peat particles per unit volume, d_p (cm) is the average particle diameter, ρ (g/cm³) is the true solid phase density and ϵ_p is the adsorbent porosity. The external mass transfer coefficient k_f can be determined from the slope of the curve C/C_0 vs. time, t .

2.5.1.6. Particle diffusion model If diffusion of Cu(II) ions through the peat is the slowest step then particle diffusion is rate limiting and may be described by Boyd et al. [47], using the following equation:

$$X(t) = 1 - \frac{6}{\pi^2} \sum_{Z=1}^{\infty} \frac{1}{Z^2} \exp \left[\frac{-Z^2 \pi^2 D_e t}{r^2} \right] \quad (14)$$

where $X(t)$ is the fractional attainment at time t , given by:

$$X(t) = \frac{q_t}{q_e} \quad (15)$$

where q_t and q_e are solute loading on the solid phase at time t (min), and when equilibrium is attained (mg/g), respectively. Assuming spherical shape sorbent, the Vermeulen's [48], approximation of Eq. (14) fits the whole range $0 < X(t) < 1$ and is given as:

$$X(t) = \left[1 - \exp \left[-\frac{\pi^2 D_e t}{r^2} \right] \right]^{1/2} \quad (16)$$

This equation could be further simplified to cover most of the data points for calculating the effective particle diffusivity using the following expression:

$$\ln \left[\frac{1}{1 - X^2(t)} \right] = \frac{\pi^2}{r^2} D_e t \quad (17)$$

A linear plot of $\ln[1/1 - X^2(t)]$ vs. t produces a straight line and thus the diffusion coefficient, D_e (cm²/min) can be calculated [49].

2.5.1.7. Biot number The dominance of film and particle diffusion may further be assessed using the Biot number. This represents the ratio of the rate of diffusion across the liquid film to the rate of diffusion within the particle and can be determined using the following expression [50]:

$$Bi = \frac{k_f R}{D_{\text{eff}}} \quad (18)$$

where k_f is the film diffusion coefficient, R (cm) is the particle radius and D_{eff} is the particle diffusion coefficient.

2.5.2. Artificial neural networks

ANNs are algorithmic systems consisting of interconnected nodes or neurons which simulate the working principle of the human brain. It has been successfully employed as predictive models in adsorption studies due to its ability to capture non-linear multivariate relationships, predict with limited numbers of experiments and its potential to learn complex relationships without knowledge of the model architecture or a mathematical description of the phenomena involved in the process [51].

In this study, a multilayer feed-forward ANN model was developed for predicting the adsorption of copper onto peat moss. A total of 102 experimental data points were used to train and test the performance of ANN for the adsorption process. Each set contains five input variables comprising; particle size (GMS 0.11–1.05 mm), agitation speed (300–900 rpm), conductivity (200–4,600 $\mu\text{S}/\text{cm}$), initial pH (2.78–6.5) and contact time (0–60 min), and one output variable, namely, the relative adsorption capacity (2.0–30.95 mg/g).

The dataset was divided where 70% of the data were applied to training the network, 15% for crossvalidation and 15% for testing the accuracy of the neural network model and its prediction. The impact of network parameters including training functions, transfer functions (Logsig, Tansig and Purelin) and hidden layer neuron number was then investigated to optimize the ANN structure.

2.5.3. Genetic algorithm

A GA is a type of global optimization technique inspired by the mechanics of natural selection and genetic evaluation [52]. This technique utilizes random search for optimizing a fitness function. Maximization or minimization is performed by applying three genetic operators (selection, crossover and mutation) and selecting the best-fitted individuals as measured by a fitness function. An initial population was first generated. The selection operator was then applied to choose the best-fitted individuals to be parents of the new generation using different methods including stochastic uniform, remainder, uniform, shift linear, roulette and tournament. Crossover operator interchanged the genes of two potential parents in an attempt to produce offsprings with positive traits of both parents and thus limiting the possibility of inheriting negative traits from either parent. This was performed using different methods including single point, double point or uniform crossover. Finally, the mutation operator changed all or some of the genes of the parents to increase the exploration of the genome such that the offsprings are not limited to the genes of the parents and may have new and better traits [53].

In this study, the optimization toolbox of MATLAB® R2012a was used to determine the optimum conditions for achieving maximum adsorption of copper onto peat moss. The resulting weights and biases of the trained ANN are considered to be the individuals in the colony, and the objective function was the equation obtained from the ANN model.

2.6. Error analysis

The goodness of fit by the various kinetic and predictive models to the experimental data were evaluated using the linear coefficient of determination, R^2 , the Marquardt's percent standard deviation (MPSD), hybrid error function (HYBRID), mean square error (MSE) and relative percentage error (RPE) are presented in Table 2.

3. Results and discussion

3.1. Kinetic studies

3.1.1. Effect of biosorbent pretreatment

Peat moss samples were subjected to hot-alkali treatment prior to biosorption. Images of untreated and treated peat presented in Figs. 1(a) and (b), respectively, reveal the success of pretreatment in removing constituents that may occlude the pores of the peat. SEM images at a 1,000 \times magnification of the raw peat (Fig. 1(c)) and the pretreated peat (Fig. 1(d)) reveals a porous morphology which remained somewhat unchanged after pretreatment, with repetition of plant structure, vessels orientation and pores of comparable shape and size. The influence of Cu(II) binding to the biomass surface caused significant changes in the surface morphology resulting in greater irregularity in the microstructure edges (Fig. 1(e)). Similar observations have been reported by Mitic-Stojanovic et al. [54], for the biosorption of metal ions onto *Lagenaria vulgaris* shell. They went on to explain that this may imply that metal binding is strongly related to the chemical composition of the biomass.

The EDS of untreated peat moss reveal the presence of C and O and trace amounts of Al, Si, S and Ca (Fig. 2(a)). After hot-alkali pretreatment using NaOH, the C, Al, Si and S peaks diminished while the Ca increased (Fig. 2(b)). Further, pretreatment revealed the appearance of Mg, Fe, Cu and Pb peaks which became significant by following the reduction in C, Al, Si and S.

After biosorption by the pretreated peat, the O, Mg, Al, Si and Pb peaks diminished whereby the Ca peak revealed a significant reduction (Fig. 2(c)). The Cu at 0.9, 8.1 and 8.9 keV peaks became increasingly visible confirming the binding of Cu(II) ions to the peat surface. Furthermore, the presence of Ca^{2+} and Mg^{2+} , which are known to be involved in the process of ion-exchange [55], was indicated in the spectra of pretreated peat moss. After the adsorption of the Cu(II), these cations diminished in the EDS of Cu(II) – loaded pretreated peat. These findings, therefore, indicate the involvement of the mechanism of ion-exchange for the removal of Cu(II) ions.

The kinetic effect of hot-alkali treatment on Cu(II) sorption is presented in Fig. 3. The plot of the primary kinetic data shows a significant improvement in performance by the hot-alkali treated sample. The treated sample attained equilibrium ~30 min into the reaction while the untreated reached equilibrium after 45 min. Lee et al. [56] reported a maximum Cu(II) adsorption by Russian peat of 18.2 mg/g after pyrolysis at 800°C. Gardea-Torresday et al. [57] worked with acid washed Canadian peat which produced a maximum sorption of 16.1 mg/g at pH 4.0. Fig. 3 reveals that for an initial concentration of 50 mg/L and at the present operational conditions the relative maximum sorption capacity was 29.9 mg/g, ~19%

Table 2
Error functions

Error functions	Expression	Eq.
Relative percentage error (RPE)	$\text{RPE \%} = \frac{\sum [(q_e)_{\text{Predicted}} - (q_e)_{\text{experimental}}] / (q_e)_{\text{experimental}}}{N} \times 100$ <p>where N is the number of experimental points</p>	(19)
Marquardt's percent standard deviation (MPSD)	$\text{MPSD} = 100 \sqrt{\frac{1}{N-P} \sum_{i=1}^N \left[\frac{(q_{e_i})_{\text{experimental}} - (q_{e_i})_{\text{Predicted}}}{(q_{e_i})_{\text{experimental}}} \right]^2}$ <p>where N is the number of experimental points and P is the number of parameters in the regression model</p>	(20)
The hybrid error function (HYBRID)	$\text{HYBRID} = \frac{100}{N-P} \sum_{i=1}^N \left[\frac{((q_{e_i})_{\text{experimental}} - (q_{e_i})_{\text{Predicted}})^2}{(q_{e_i})_{\text{experimental}}} \right]$ <p>where N is the number of experimental points and P is the number of parameters in the regression model</p>	(21)
R^2	$R^2 = \frac{\sum_{i=1}^N (t_i - t_{\text{mean}})^2 - \sum_{i=1}^N (t_i - y_i)^2}{\sum_{i=1}^N (t_i - y_i)^2}$ <p>where N is the number of experimental points, t_{mean} is the mean target value, t is the target (experimental) data and y is the predicted value</p>	(22)
MSE	$\text{MSE} = \left(\frac{1}{n} \sum_{i=1}^n [t_i - y_i]^2 \right)$ <p>where N is the number of experimental points, t is the target (experimental) data, and y is the predicted value</p>	(23)

higher than that of the untreated sample. This improvement may be due to greater access to previously unavailable sites within the peat created by the chemical pretreatment.

Kinetic simulation of peat moss biosorption was attempted using four models: Lagergren model [39]; pseudo-second-order model [40]; Weber and Morris intraparticle diffusion model [42]; and the diffusion–chemisorption model [44]. Table 3 shows the results of linear and non-linear regression for untreated and treated peat moss, respectively. The goodness of fit was assessed using error functions presented in Table 2. These error functions were determined by comparing primary experimental curves with non-linear curves generated using the calculated equation parameters.

Linear regression of both treated and untreated samples revealed a relatively poor simulation by the pseudo-first-order and the intraparticle diffusion model. The pseudo-second-order model produced the highest correlation to the untreated sample while the diffusion–chemisorption model best represented the treated peat sample. Kinniburgh as cited in [58], highlighted that the transformation of a non-linear model to a linear form could implicitly alter the error functions as well as the error variance and normality assumptions of the least squares methods. Consequently, a more robust simulation was performed using non-linear regression by the Levenberg–Marquardt algorithm [59]. The result verifies the findings of the linear regression and is presented in Table 3.

3.1.2. Effect of agitation on biosorption

The kinetic effect of variations in agitation speed on the sorption of Cu(II) onto peat moss is presented in Fig. 4. These experiments were conducted with particles of GMS 0.65 mm and pH of 5.5. The plot shows the effect of mixing speed on the overall and initial reaction rate obtained from the diffusion–chemisorption kinetic model. Increased agitation promotes good contact between the media and liquid. Additionally, it reduces the thickness of the solvent film surrounding the particle and thus reduces the resistance by film diffusion. At higher agitation speed, a positive effect on intraparticle diffusion is expected due to the maintenance of a high ion concentration gradient between the inner and outer regions of the particle. Analysis of the curve supports this view as it can be seen that an increase in initial and overall adsorption rate occurs as the mixing speed is increased. This was further accompanied by a decrease in the time to reach equilibrium and as a consequence may have accelerated the onset of intraparticle resistance.

3.1.3. Effect of pH on biosorption

The effect of solution pH on the biosorption kinetics of Cu(II) and Pb(II) by peat moss was studied. Experiments were carried out with solution pH varying from 2.5 to 6.0 and using a particle GMS of 0.65 mm and initial concentration of

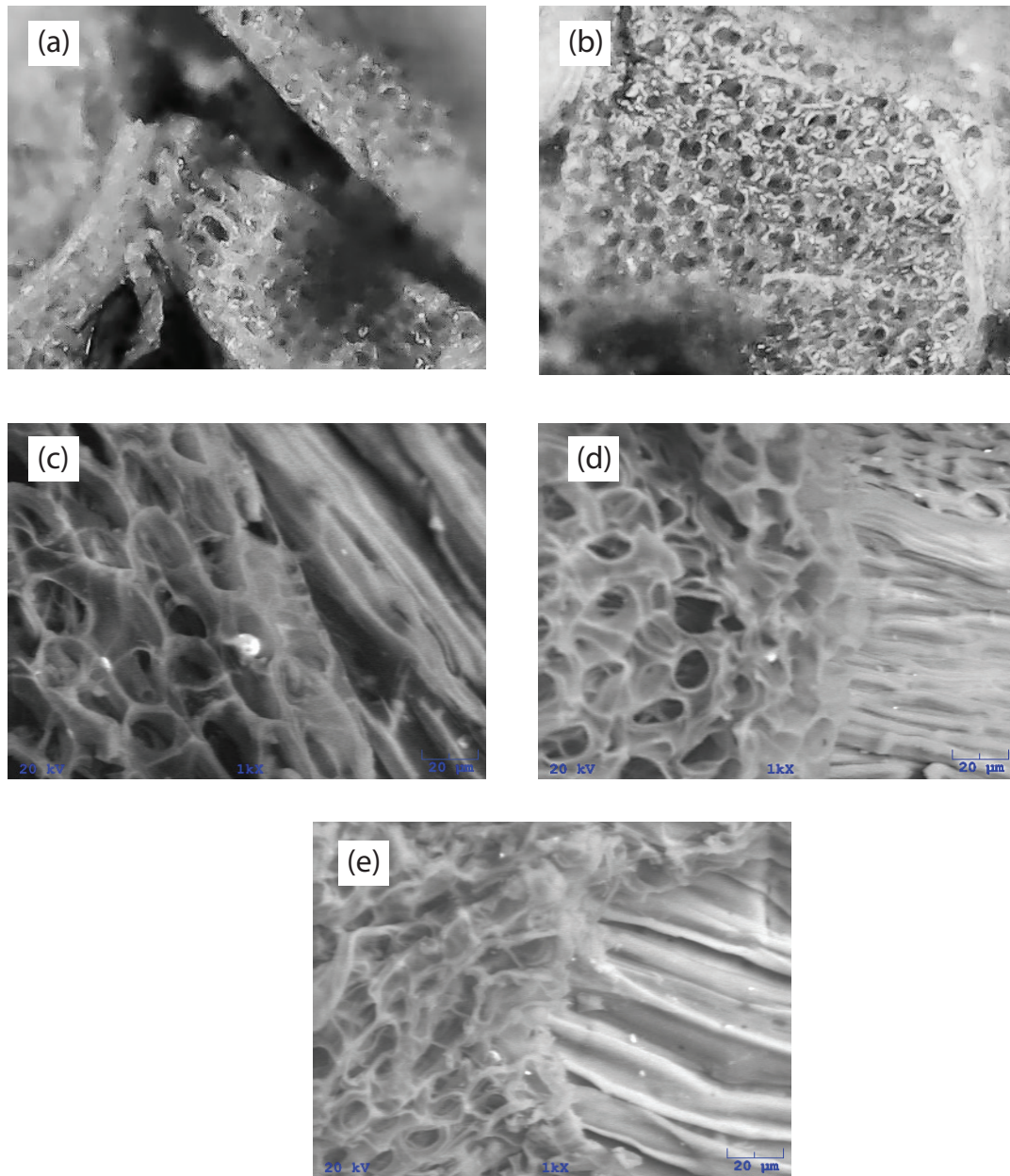


Fig. 1. (a) Micrograph image of untreated peat moss (200 \times). (b) Micrograph image of hot-alkali treated peat moss (200 \times). (c) Micrograph image of untreated peat moss (1,000 \times). (d) Micrograph image of hot-alkali treated peat moss (1,000 \times). (e) Micrograph image of hot-alkali treated peat moss loaded with Cu(II) ions (1,000 \times).

50 mg/L. Solution pH has been identified in the literature as a crucial parameter in adsorption processes and is verified here as one of the most important variables governing metal biosorption onto peat moss. The curves in Fig. 5 show that at an initial concentration of 50 mg/L, optimum removal was achieved at a pH of 5.5. The minimal observed performance at pH 2.5 may be partly due to the fact that hydrogen ions themselves are strong competing adsorbates.

Additionally, the solute pH can influence the speciation of metal ions and the ionization of surface functional groups. Elliot and Huang as cited in [60], explained that at pH 6.0 there exist three copper species, Cu(II) in very small quantity and Cu(OH)⁺ and Cu(OH)₂ in large quantities. The reduction

in sorption observed at pH 6.0 may indicate a preference by peat moss for the Cu(II) ions over that of the other species. A similar analysis of Pb(II) sorption by peat moss within the pH range of 2.5–6 (results not shown) indicated that optimum sorption occurred at pH 4.0. At a pH below 4.0, a decrease in sorption was observed possibly due to competition between H⁺ ions and the metal ions for the same functional groups. A similar trend was reported by El-Said [61], for the biosorption of Pb(II) onto rice husk and its ash. At higher pH, a decrease in sorption was observed. Baes and Mesmer [62] reported that the hydrolysis and precipitation of the hydroxide form which occurs at pH > 6 might account for this reduction in sorption.

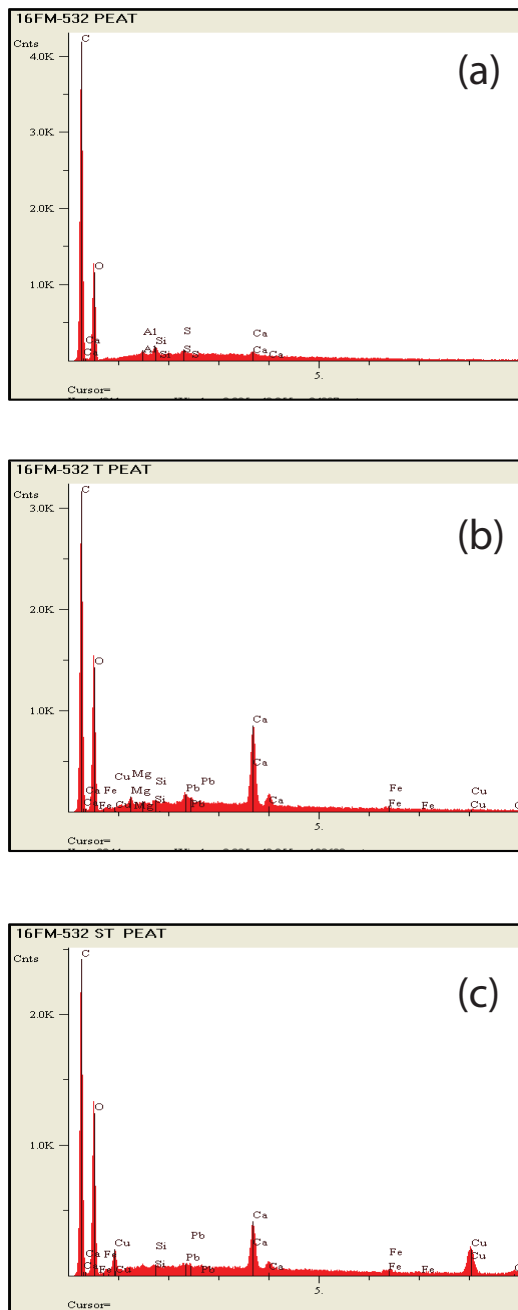


Fig. 2. (a) Energy dispersive spectrum of untreated peat moss. (b) Energy dispersive spectrum of hot-alkali treated peat moss. (c) Energy dispersive spectrum of hot-alkali treated peat moss loaded with Cu(II) ions.

3.1.4. Effect of particle size on biosorption

The influence of the peat moss particle size on biosorption kinetics was studied in single-component batch reaction using Cu(II) ions and Pb(II) ions. Table 4 presents the results of non-linear regression analysis using the diffusion–chemisorption model. From the table, it is observed that as particle size decreased, both the overall rate and the initial rate increased. This trend was observed for both Cu(II) and Pb(II) biosorption. If the primary kinetic data are linearized

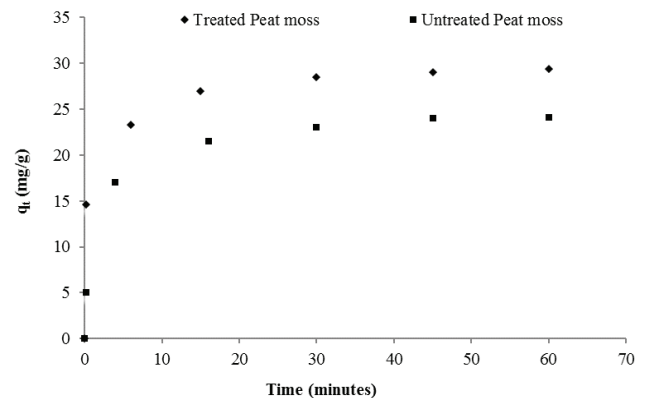


Fig. 3. Primary kinetic curve depicting the sorption of Cu(II) onto untreated and treated peat moss.

by a plot of $\log q_t$ against $\log t$ as observed in Figs. 6(a) and (b), the plots eventually converge, indicating that the metal ion capacity is independent of particle size, and thus, there is no occlusion of internal sites within the pore of the sorbent. At a particle GMS of 0.21 mm, initial concentration of 50 mg/L, solution pH of 5.2, agitation of 300 rpm and conductivity of 1,045 $\mu\text{S}/\text{cm}$, the highest observed Cu(II) uptake was 28.5 mg/g, while 39.5 mg/g was observed for Pb(II) at a pH of 4.0. It may then be reasonable to assume that the difference in sorption capacity between Cu(II) and Pb(II) may in part be influenced by their atomic weights and differences in ionic radius. Similar observations were reported by Jiang et al. [63], for the adsorption of copper, lead, zinc and cadmium ions onto tourmaline as well as Cheng et al. [64], for adsorption of heavy metals onto magnetotactic bacteria.

3.1.5. Effect of electrical conductivity on biosorption

Primary data obtained from batch experiments of varying solution electrical conductivity (EC) were analyzed using the diffusion–chemisorption model, and the parameters are presented in Table 5. The results indicate that adsorption capacity was unaffected up to an EC of 4,600 $\mu\text{S}/\text{cm}$. This was probably due to the strong affinity for divalent ions over the monovalent ions at the charged interface [65]. At an EC of 15,000 $\mu\text{S}/\text{cm}$, there was a 20% observed reduction in sorption capacity and 30% reduction in overall reaction rate. As EC increases, the amount of electrolyte present in the solution can swamp the surface of adsorbents, thus decreasing the access of metal ions to the adsorbent surface. This is particularly important when electrostatic attraction is a significant mechanism for metal removal.

3.1.6. Interruption test

Intraparticle diffusion within porous particles is based on pore and solid diffusion [66]. Tests on the variation in particle size showed that the rate of adsorption increased with a decrease in size and that sorption capacity is independent of particle size; this confirms the presence of pore diffusion. The interruption test was conducted to determine the presence of diffusion in the adsorbed state by surface migration. Fig. 7 shows an increase in uptake of ~3.5% after 10 min of process

Table 3
Analysis of kinetic models using linear and non-linear regression for Cu(II) uptake by untreated peat moss and treated peat moss

Metal ion	Regression	Model	Error functions			
			RPE	MPSD	HYBRID	R ²
Untreated peat moss	Linear	Pseudo-first-order	39.025	56.850	429.121	0.9420
		Pseudo-second-order	4.520	8.383	6.680	0.9990
		Intraparticle diffusion	29.212	45.657	283.024	0.8222
		Diffusion–chemisorption	9.434	28.420	40.757	0.9551
	Non-linear	Pseudo-first-order	13.235	30.485	50.477	0.9768
		Pseudo-second-order	5.101	11.749	7.962	0.9937
		Intraparticle diffusion	30.715	45.529	259.494	0.7049
		Diffusion–chemisorption	5.348	13.059	9.651	0.9928
Treated peat moss	Linear	Pseudo-first-order	45.037	63.000	845.826	0.9537
		Pseudo-second-order	17.975	32.241	177.117	0.9985
		Intraparticle diffusion	38.640	56.279	653.073	0.7559
		Diffusion–chemisorption	15.969	23.273	110.379	0.9900
	Non-linear	Pseudo-first-order	5.849	10.053	24.830	0.9653
		Pseudo-second-order	5.099	9.737	21.504	0.9753
		Intraparticle diffusion	34.932	53.189	529.336	0.3952
		Diffusion–chemisorption	3.247	6.117	8.069	0.9949

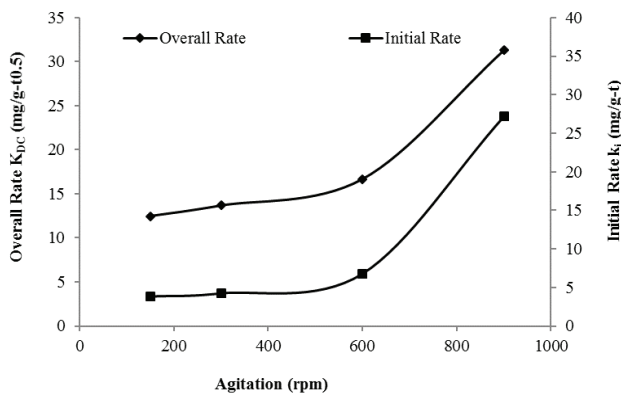


Fig. 4. Effect of agitation on the kinetic parameters for Cu(II) uptake by peat moss.

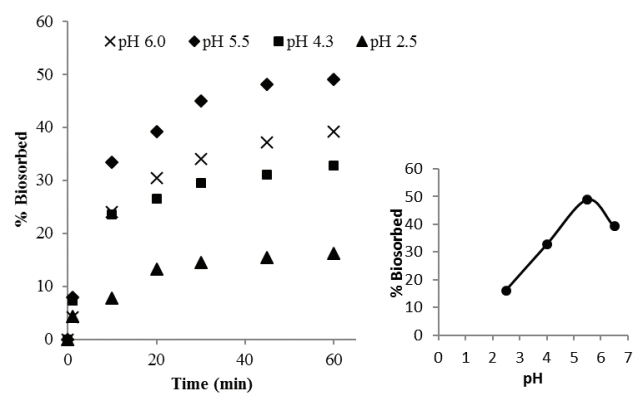


Fig. 5. Effect of solution pH on Cu(II) uptake by peat moss.

interruption. Further, as a result of process interruption, it was also observed that the time to reach equilibrium was reduced. It can, therefore, be surmised that solid-state diffusion is an operative mechanism in the adsorption process.

3.2. Elucidation of mechanisms of biosorption

Ho et al. [67], in their review of the kinetics of pollutant sorption by biosorbents, explained that external film diffusion is best identified by carrying out a series of agitated batch contact time experiments at different agitation speeds. Sağ and Aktay [68] successfully explored this effect of agitation on film diffusion by the use of the Reynolds number for sorption of chromium ions onto chitin and concluded that increased turbulence reduces the film boundary layer surrounding the

Table 4
Diffusion–chemisorption parameters for Cu(II) and Pb(II) uptake by varying particle size

Adsorbate	Particle size GMS (mm)	K _{DC} (mg/g t ^{0.5})	k _i (mg/g t)	R ²
Cu(II)	0.11	35.204	36.602	0.9942
	0.21	16.158	6.846	0.9927
	0.65	9.214	2.191	0.9993
	1.05	5.211	0.460	0.9986
Pb(II)	0.21	12.750	10.966	0.9858
	0.65	7.128	0.471	0.9754
	1.05	5.383	0.142	0.9800

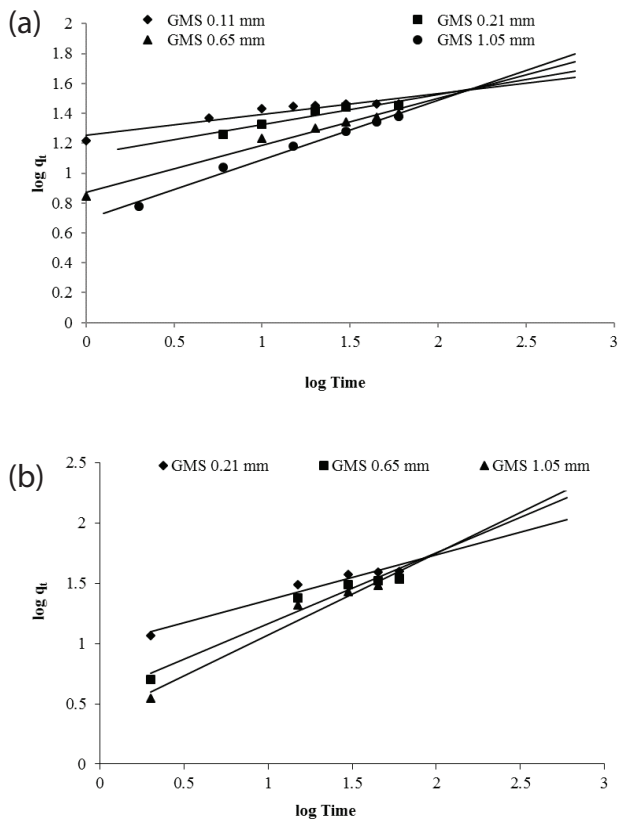


Fig. 6. (a) Log–log plot of Cu(II) uptake by peat moss for various particle size. (b) Log–log plot of Pb(II) uptake by peat moss for various particle size.

Table 5
Diffusion–chemisorption parameters for Cu(II) uptake by varying electrical conductivity

EC ($\mu\text{S}/\text{cm}$)	q_e (mg/g)	K_{DC} (mg/g $t^{0.5}$)	k_i (mg/g t)	R^2
1,045	29.905	12.524	5.245	0.9798
4,600	29.880	10.911	3.984	0.9977
15,000	23.693	7.682	2.491	0.9618

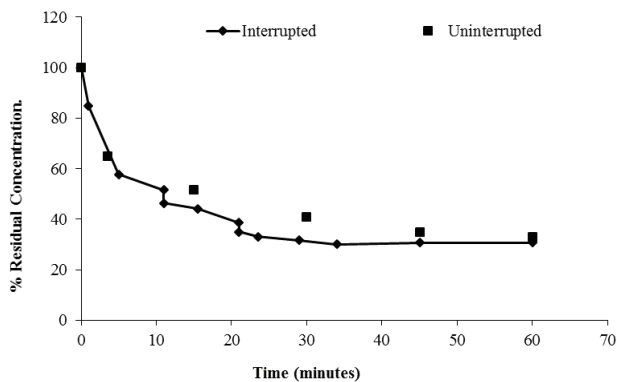


Fig. 7. Effect of process interruption on the uptake of Cu(II).

absorbent. In this study, the observed changes in sorption rate due to variation in agitation have confirmed the presence of film diffusion on the reaction kinetics. Initial and overall reaction rates were found to vary inversely with particle size. Since the sorption capacity was shown to be independent of particle size, pore diffusion was confirmed as an operative mechanism. The other component of intraparticle diffusion, that is, solid diffusion was confirmed by the interruption test to be influential in process reaction.

The single-resistance intraparticle diffusion model described by Weber and Morris, suggest that if the adsorption process is influenced by intraparticle diffusion, the adsorbed amount, q_t should vary linearly with the square root of time. Fig. 8 depicts a plot of the Weber and Morris model for two particle sizes namely GMS 0.21 and 1.05 mm. In both instances, the plots did not go through the origin. It was also observed that as particle size reduces (which accompanies an increase in surface area and reduction in pore length), the plot moves further from the origin. Several studies [43,69,70] have reported that this increase in intercept reveals the growing effect of the boundary layer. The plot of GMS 0.21 mm shows two distinct slopes. The first slope, which occurs from 1 to 10 min reveals the impact of intraparticle diffusion which may be rate controlling. Some researchers have reported that the final slope corresponds to the slowing of the reaction, possibly due to a reduction in concentration gradient as the reaction approaches equilibrium [71,72]. The plot of GMS 1.05 mm reveals the increased dominance over most of the reaction period by intraparticle diffusion as the particle size was increased. Similar behaviour has been reported by Choy et al. [73], for the adsorption of cadmium onto various particle sizes of bone char. Based on the preceding analysis it is evident that both film and intraparticle diffusion has some amount of influence on the rate-determining step. To further explicate this phenomenon the external diffusion and particle diffusion models were fitted with the experimental data. The resulting mass transfer coefficients were used to calculate the Biot number and assess the relative importance of external diffusion to intraparticle diffusion with changing particle size. The Biot number is a good indicator of which phase controls the rate of mass transfer. For values <1.0 , external mass transfer controls the biosorption rate. For large Biot numbers (>30), surface diffusion controls the biosorption rate. For numbers between

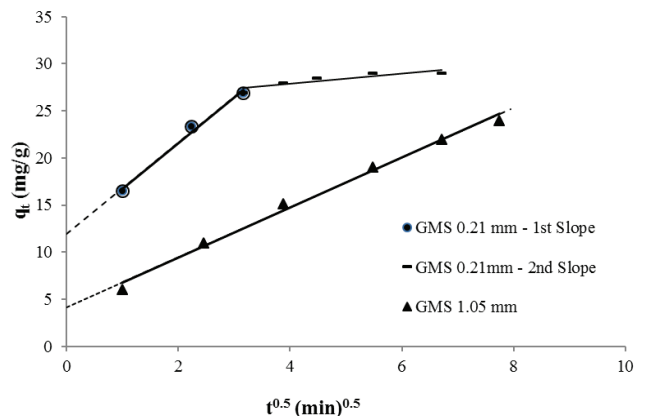


Fig. 8. Kinetic plot of intraparticle diffusion model for various particle size.

1 and 30, both external and intraparticle mass transfer rates contribute to the adsorption rate [74]. As particle size increased the Biot numbers also increased (Table 6). For particles beyond GMS 0.65 mm intraparticle diffusion becomes the dominant rate-limiting step. Evaluating the rate-limiting mechanisms can present practical options to improve biosorption. When film diffusion is limiting, one should improve mixing/turbulence. If intraparticle diffusion is rate limiting then smaller biosorbent particles should be used [75].

3.3. Development of a predictive model

3.3.1. Optimization of ANN structure

The optimization of a neural network plays an important role in the performance of the network [76]. In this study, the optimum architecture of the ANN model was determined by assessing the impact of parameter variations on the MSE of the training and validation set. An optimization protocol was developed and is presented herein.

The impact of 13 backpropagation algorithms on the MSE was first assessed to select the best algorithm for training the network (Table 7). Using the Tansig and Purelin transfer functions at the hidden and output layer, respectively, and 10 neurons at the hidden layer, the Levenberg–Marquardt algorithm

produced the lowest MSE of 2.0571 and highest R^2 of 0.9915. The impact of transfer functions at the hidden and outer layer was subsequently assessed. This was performed using three popular transfer functions (Logsig, Tansig and Purelin) and by training the network using the Levenberg–Marquardt algorithm with 10 neurons at the hidden layer. The lowest MSE values were obtained using a Tansig transfer function at the hidden layer and a Purelin transfer function at the outer layer (Table 8). Finally, using the best algorithm and transfer functions, optimization was performed between the number of neurons in the hidden layer and the MSE. In this study, overfitting of the data was prevented by implementing the early stopping technique based on dividing the data into three subsets. According to Yetilmezsoy [77], when the network begins to overfit the data, the error on the validation set usually start to rise. The training subset was used for calculating the gradient and updating the network weights and biases. To prevent overfitting, the error on the validation subset was monitored, and training was terminated at the minimum value [78]. The results presented in Fig. 9 indicated that the lowest MSE was obtained using 20 neurons in the hidden layer.

The characteristics of the optimized ANN are presented in Table 9, and a schematic representation of the architecture is shown in Fig. 10. A comparison of the ANN predicted data and the experimental data are presented in Fig. 11. The plot shows high correlation ($R^2 = 0.9965$) between the predicted and the experimental data which highlights the accuracy of the ANN model.

Table 6
Mass transfer coefficients and Biot numbers for the biosorption of Cu(II)

Particle GMS (mm)	External diffusion model		Particle diffusion model		Biot number Bi
	k_f (cm/min)	R^2	D_e (cm ² /min)	R^2	
0.11	3.33E-04	0.3441	4.85E-07	0.9965	3.7736
0.21	2.31E-05	0.5829	1.02E-06	0.9973	23.7253
0.65	6.02E-03	0.7554	5.24E-06	0.9971	37.2845
1.05	1.07E-02	0.9054	1.10E-05	0.9808	50.6913

3.3.2. Formulation of empirical equation

The weights of the optimized ANN model and the transfer function were used to develop an empirical expression for predicting adsorption kinetics without the need to use ANN software (Eq. (24)). This empirical equation successfully incorporates the non-linear relationship of multiple batch operational parameters. Consequently, this ability to predict the overall behaviour of the process makes it a valuable tool to scale-up batch processes from laboratory data.

Table 7
Comparison of various backpropagation algorithms

Backpropagation (BP) algorithms	Function	MSE	IN	R^2
BFGS quasi-Newton backpropagation	Trainbfg	17.0961	12	0.7311
Powell–Beale conjugate gradient backpropagation	Traincgb	28.8950	15	0.7418
Fletcher–Reeves conjugate gradient backpropagation	Traincgf	6.2600	42	0.9361
Polak–Ribiere conjugate gradient BP	Traincgp	22.5300	16	0.7442
Gradient descent	Traingd	279.4313	6	0.0863
Gradient descent with momentum	Traingdm	279.4313	6	0.0863
Gradient descent with adaptive learning rate	Traingda	45.4966	21	0.4652
Gradient descent with momentum and adaptive learning	Traingdx	42.2333	25	0.3002
Levenberg–Marquardt backpropagation	Trainlm	2.0571	52	0.9915
One step secant backpropagation	Trainoss	27.7438	12	0.6357
Resilient backpropagation	Trainrp	31.2997	16	0.7250
Scaled conjugate gradient backpropagation	Trainscg	26.2069	16	0.7306

IN, Iteration Number; BFGS, Broyden–Fletcher–Goldfarb–Shanno.

$$\begin{aligned}
 q_{i \text{ pred}} = & 0.0766F_1 + 0.9665F_2 + 0.7122F_3 - 2.6940F_4 \\
 & + 1.1595F_5 - 0.3087F_6 + 0.1046F_7 + 0.6258F_8 \\
 & + 0.7452F_9 + 0.0773F_{10} - 0.2281F_{11} + 0.5348F_{12} \\
 & - 0.8156F_{13} - 0.6194F_{14} - 0.0100F_{15} + 0.1756F_{16} \\
 & - 0.0745F_{17} + 0.3614F_{18} - 0.0313F_{19} - 0.2374F_{20} \\
 & - 1.7986
 \end{aligned} \quad (24)$$

where F_i is the Tansig activation function used at the hidden layer and is given by Eq. (25):

$$F_i = \frac{2}{1 + \exp(-2 \times E_i)} - 1; \quad i = 1:20 \quad (25)$$

The input data were normalized in the range -1 to 1 using Eq. (26):

$$X_{\text{norm}} = 2 \left[\frac{X_i - X_{\min}}{X_{\max} - X_{\min}} \right] - 1 \quad (26)$$

where X_i is the input or output variable X , and X_{\min} and X_{\max} are the minimum and maximum value of variable X .

Table 8
Impact of varying transfer function on ANN structure

Activation function layer 1	Activation function layer 2	MSE (first training)	MSE (second training)
Logsig	Logsig	38.8626	30.9762
Logsig	Purelin	1.9932	0.45684
Logsig	Tansig	3.3989	0.54762
Purelin	Logsig	22.4315	41.4193
Purelin	Purelin	19.6998	14.1929
Purelin	Tansig	11.3439	19.4231
Tansig	Logsig	36.4061	30.5938
Tansig	Purelin	2.0571	0.1361
Tansig	Tansig	1.0849	0.30369

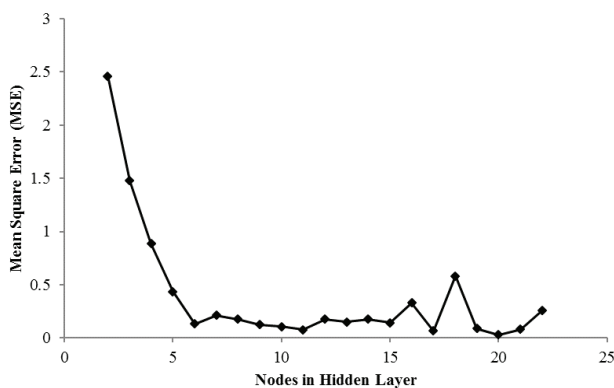


Fig. 9. Effect of the number of neurons in the hidden layer on ANN performance.

E_i is the weighted sum of the normalized input calculated using values from Table 9 and is defined as follows:

$$E_i = W_{i1} \times \text{pH} + W_{i2} \times d_p + W_{i3} \times \text{RPM} + W_{i4} \times \text{EC} + W_{i5} \times t + b_i \quad (27)$$

3.3.3. Sensitivity analysis

The influence of input parameters on the adsorption of copper onto peat moss was quantitatively determined using the weight method proposed by Garson [79] and is presented as Eq. (28):

$$I_j = \frac{\sum_{m=1}^{m=N_h} \left(\left(|W_{jm}^{ih}| \div \sum_{k=1}^{N_i} |W_{km}^{ih}| \right) \times |W_{mn}^{ho}| \right)}{\sum_{k=1}^{k=N_i} \left\{ \sum_{m=1}^{m=N_h} \left(|W_{km}^{ih}| \div \sum_{k=1}^{N_i} |W_{km}^{ih}| \right) \times |W_{mn}^{ho}| \right\}} \quad (28)$$

where I_j is the relative importance of the j th input variable on the output variable, N_i and N_h are the numbers of input and hidden neurons, respectively. W is connection weight, the superscripts i , h and o refer to input, hidden and output layers, respectively. Subscripts k , m and n refer to input, hidden and output neurons, respectively.

Using Eq. (28), reaction time was found to be the most influential parameter in the adsorption process with a relative importance of 30%. This was followed by particle size (23%), conductivity (18%), agitation (17%) and finally pH (12%). The importance of reaction time was expected, as increasing contact time between adsorbate and adsorbent enhances the probability of collision of the adsorbate onto a sorption site.

3.3.4. Genetic algorithm optimization

After the ANN model was developed, the input space was optimized using the GA technique to determine the

Table 9
Optimum ANN structure

Type	Details
Network type	Feed-forward backpropagation
Transfer function (hidden layer)	Tansig
Transfer function (output layer)	Purelin
Training function	Levenberg–Marquardt
Performance function	Mean square error (MSE)
Neurons in input layer	5
Neurons in hidden layer	20
Neurons in output layer	1
Data used for training	70%
Data for crossvalidation	15%
Data for testing	15%

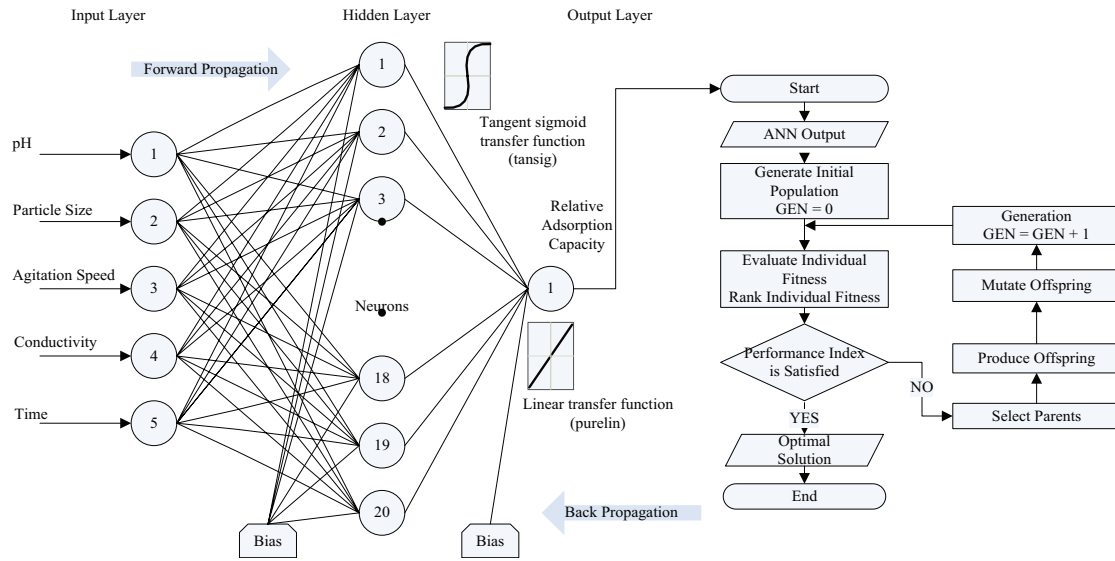


Fig. 10. Architecture of ANN-GA.

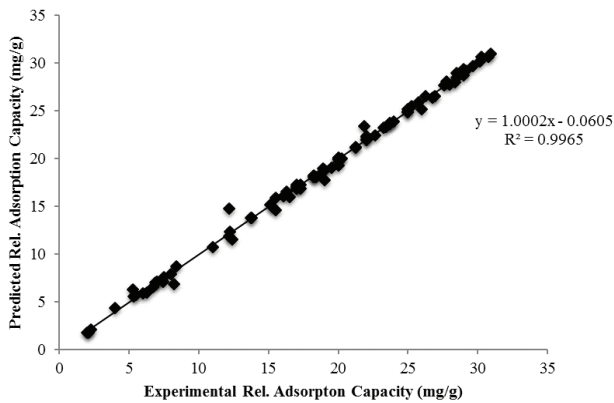


Fig. 11. Comparison of experimental and predicted adsorption capacity by ANN model.

optimum conditions (pH, particle size, agitation, conductivity and time) necessary for maximizing biosorption. The equation obtained from the ANN model was used as the objective function [35], and can be represented as follows:

$$\text{Objective function} = \text{purelin}(LW \times \text{tansig}(IW \times [x(1);x(2);x(3);x(4);x(5)] + b1) + b2) \quad (29)$$

where IW and b1 are the weight and bias of the hidden layer and LW and b2 are the weight and bias of output layers from Table 10.

A double vector population type was selected, and the population size, population generation, crossover fraction and mutation rate were set to be 100, 100, 0.7 and 0.01, respectively. The selection, crossover and mutation operators were chosen as stochastic uniform, two point and uniform, respectively. Fig. 12 presents the fitness values vs. generation. After ~40 generations, the value of fitness reached a minimum and then remained constant. The ANN-GA optimization indicated that

maximum sorption could be obtained using pH 5.5, particle size 0.21 mm, agitation 690 rpm, conductivity 290 $\mu\text{S}/\text{cm}$ and contact time 50 min. The model prediction of the relative sorption capacity under these optimized conditions was 32.25 mg/g. The accuracy of the ANN-GA was then validated by conducting experimental biosorption kinetics using the optimized operational parameters. The resulting relative sorption capacity was 31.37 mg/g producing a residual error of 2.8%, thus revealing an excellent prediction by the ANN-GA model and bolsters its usefulness in engineering applications.

4. Conclusions

Batch biosorption kinetic studies were carried out to assess the improved performance of chemically treated peat moss. Hot-alkali pretreatment of peat moss resulted in a 19% increase in relative sorption capacity over that of the untreated sample and compares well to other previously reported methods. The positive impact of hot-alkali treatment is attributed to a reduction in the occlusion of pores within the peat structure which resulted in an increased rate and uptake capacity. Experimentally, operational parameters were varied and analyzed using theoretical kinetic models. The reaction kinetics was well represented by the diffusion-chemisorption model.

The rate-limiting steps involved in the process of biosorption included film diffusion followed by intraparticle diffusion and was dependent on biosorbent size. At the given operational parameters, the solution pH influenced the speciation of metal ions which in turn affected the biosorption process. Competing ions in solution had an insignificant effect up to an EC of 4,600 $\mu\text{S}/\text{cm}$. Beyond this value, a significant decrease in sorption capacity and reaction rate was observed.

A predictive model to simulate the kinetic process was successfully developed using an ANN and optimized using a GA. The optimum parameters predicted by the GA were subsequently validated by additional experimental studies

Table 10
Weight and bias values obtained by the Levenberg–Marquardt algorithm with 20 neurons

	Input 1 (pH)	Input 2 (dp)	Input 3 (RPM)	Input 4 (Cond)	Input 5 (<i>t</i>)	Bias 1	Output
Node 1	-0.1545	0.8092	-0.0676	1.2704	-0.0728	-2.9460	0.0766
Node 2	0.8561	-1.8849	-2.6172	1.7427	-0.6955	-2.1092	0.9665
Node 3	0.4082	4.3623	0.7753	-1.5454	-0.1091	1.6982	0.7122
Node 4	0.1927	-0.1068	0.0318	-0.0158	-4.3706	-5.3802	-2.6940
Node 5	-0.0008	-0.3467	-1.6784	3.0803	-0.1762	-1.1702	1.1595
Node 6	-3.4976	0.6831	0.1732	1.0686	-1.8171	0.0329	-0.3087
Node 7	-4.9724	0.7190	-2.1273	0.1404	2.7533	-0.7309	0.1046
Node 8	0.5366	-5.6794	4.1767	0.3160	0.9517	-1.1740	0.6258
Node 9	0.0704	2.0166	0.5886	-2.1136	0.8044	0.4143	0.7452
Node 10	1.3470	-1.1325	-0.7122	-0.4996	-0.1672	2.1200	0.0773
Node 11	-2.1754	1.1831	0.2953	-0.0488	1.7623	0.0075	-0.2281
Node 12	1.3694	-3.2031	0.3063	-1.7548	-0.0872	1.3357	0.5348
Node 13	1.8972	0.9376	2.2764	1.7740	-0.3760	0.9680	-0.8156
Node 14	-0.3233	-2.4976	-2.2798	0.5602	-0.2359	0.5413	-0.6194
Node 15	2.0369	-0.6471	1.2176	4.0817	-0.4771	-2.1193	-0.0100
Node 16	-3.7020	5.3290	-1.2492	-0.5042	-1.4657	-2.8242	0.1756
Node 17	-0.6127	1.0656	1.7640	-0.5247	0.4279	-2.5638	-0.0745
Node 18	3.3359	-1.3391	0.9035	-0.4662	0.5458	-0.6731	0.3614
Node 19	0.6163	0.6947	2.6325	1.5763	-5.8130	1.3300	-0.0313
Node 20	1.3743	-1.6192	-1.0876	-0.2713	-0.3377	2.7698	-0.2374
Bias 2							-1.7986

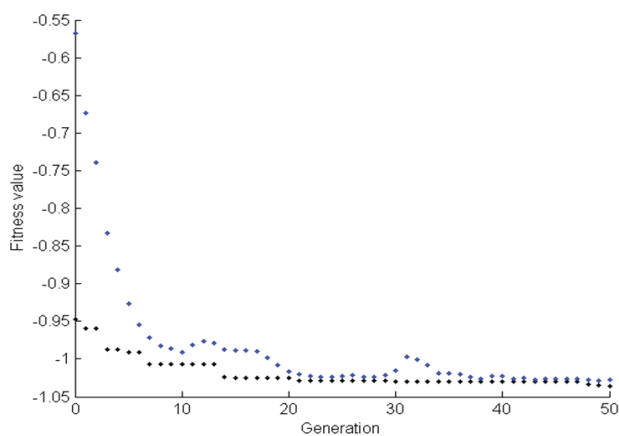


Fig. 12. Fitness values vs. generation.

which revealed a minimal residual error of 2.8%. Therefore, the non-linear relationships exhibited by the process variables were successfully captured by the model. Consequently, the high predictive capability of the model can reduce laboratory experimentation, as well as predict the performance, and aid in the design of scaled-up batch treatment system.

References

- [1] J.S. Ogola, W.V. Mitullah, M.A. Omulo, Impact of gold mining on the environment and human health: a case study in the Migori gold belt, Kenya, *Environ. Geochem. Health*, 24 (2002) 141–157.
- [2] J. Lebel, D. Mergler, F. Branches, M. Lucotte, M. Amorim, F. Larribe, J. Dolbec, Neurotoxic effects of low-level methylmercury contamination in the Amazonian Basin, *Environ. Res.*, 79 (1998) 20–32.
- [3] US Environmental Protection Agency, Final Report: Integrated Science Assessment for Lead, USEPA, Washington, D.C., USA, EPA/600/R-10/075F, 2013.
- [4] R. Saravanane, V.V. Ranade, V.M. Bhandari, A.S. Rao, Urban Wastewater Treatment for Recycling and Reuse in Industrial Applications: Indian Scenario, *Industrial Wastewater Treatment, Recycling and Reuse*, Butterworth-Heinemann, Oxford, 2014, pp. 283–322.
- [5] S.M. Shaheen, F.I. Eissa, K.M. Ghanem, H.M.G. El-Din, F.S. Al Anany, Heavy metals removal from aqueous solutions and wastewaters by using various by products, *J. Environ. Manage.*, 128 (2013) 514–521.
- [6] F. Fu, Q. Wang, Removal of heavy metal ions from wastewaters: a review, *J. Environ. Manage.*, 92 (2011) 407–418.
- [7] M. Owlad, M.K. Aroua, W.A.W. Daud, S. Baroutian, Removal of hexavalent chromium-contaminated water and wastewater: a review, *Water Air Soil Pollut.*, 200 (2009) 59–77.
- [8] G. McKay, S.J. Allen, I.F. McConvey, M.S. Otterburn, Transport processes in the sorption of colored ions by peat particles, *J. Colloid Interface Sci.*, 80 (1981) 323–339.

- [9] M. Tsezos, B. Volesky, Biosorption of uranium and thorium, *Biotechnol. Bioeng.*, 23 (1981) 583–604.
- [10] A.K. Bhattacharya, C. Venkobachar, Removal of cadmium (II) by low cost adsorbents, *J. Environ. Eng.*, 110 (1984) 110–122.
- [11] B. Volesky, I. Prasetyo, Cadmium removal in a biosorption column, *Biotechnol. Bioeng.*, 43 (1994) 1010–1015.
- [12] A.M. Farhan, A.H. Al-Dujaili, A.M. Awwad, Equilibrium and kinetic studies of cadmium(II) and lead(II) ions biosorption onto *Ficus carcia* leaves, *Int. J. Ind. Chem.*, 4 (2013) 24–32.
- [13] T.R. Muraleedharan, C. Venkobachar, Mechanism of biosorption of copper (II) by *Ganoderma lucidum*, *Biotechnol. Bioeng.*, 35 (1990) 320–327.
- [14] L. Philip, L. Iyengar, C. Venkobachar, Evaluation of Sodium Alginate as an Immobilization Matrix for the Removal of Copper by *Pseudomonas aeruginosa*, *Proc. 9th International Symposium: Heavy Metals in the Environment*, Toronto, Canada, 1993.
- [15] G.M. Gadd, Biosorption: critical review of scientific rationale, environmental importance and significance for pollution treatment, *J. Chem. Technol. Biotechnol.*, 84 (2009) 13–28.
- [16] Y.J.P. Poots, G. McKay, J. Healy, The removal of acid dye from effluent using natural adsorbents – I peat, *Water Res.*, 10 (1976) 1061–1066.
- [17] B. Allard, K. Hakanson, S. Karlson, The Importance of Sorption Phenomena in Relation to Trace Element Speciation and Mobility, L. Landner, Ed., *Speciation of Metals in Water Sediment and Soil Systems; Proceedings of an International Workshop*, Springer-Verlag, New York, 1986, pp. 141–153.
- [18] E.R.I.C.H. Adler, K. Lundquist, Spectrochemical estimation of phenylcoumaran elements in lignin, *Acta Chem. Scand.*, 17 (1963) 13–26.
- [19] C. Caramalău, L. Bulgariu, M. Macoveanu, Cobalt (II) removal from aqueous solutions by adsorption on modified peat moss, *Chem. Bull. "POLITEHNICA" Univ. Timisoara*, 54 (2009) 13–17.
- [20] S.J. Lee, J.H. Park, Y.T. Ahn, J.W. Chung, Comparison of heavy metal adsorption by peat moss and peat moss-derived biochar produced under different carbonization conditions, *Water Air Soil Pollut.*, 226 (2015) 2106–2116.
- [21] H. Šillerová, M. Komárek, New Low Cost Sorbents for Cr(VI) – Batch and Column Experiments, *Proc. 16th International Conference on Heavy Metals in the Environment*, E3S Web of Conferences, EDP Sciences, 2013.
- [22] H. Qiu, L. Lv, B.C. Pan, Q.J. Zhang, W.M. Zhang, Q.X. Zhang, Critical review in adsorption kinetic models, *J. Zhejiang Univ. Sci. A*, 10 (2009) 716–724.
- [23] G. Naja, V. Diniz, B. Volesky, Predicting Metal Biosorption Performance, S.T.L. Harrison, D.E. Rawlings, J. Peterson, Eds., *Proc. 16th International Biohydrometallurgy Symposium*, Compress Co., Cape Town, South Africa, 2005, pp. 553–562.
- [24] S. Saraf, V.K. Vaidya, Statistical optimization of biosorption of Reactive Orange 13 by dead biomass of *Rhizopus arrhizus* NCIM 997 using response surface methodology, *Int. J. Ind. Chem.*, 6 (2015) 93–104.
- [25] P. Kumar, P. Sharma, Artificial neural networks – a study, *Int. J. Emerging Eng. Res. Technol.*, 2 (2014) 143–148.
- [26] W.S. McCulloch, W.A. Pitts, A logical calculus of the ideas immanent in nervous activity, *Bull. Math. Biol.*, 52 (1990) 99–115 (Reprinted from *Bull. Math. Biophys.*, 5 (1943) 115–133).
- [27] T.H. Kim, Pattern Recognition Using Artificial Neural Network: A Review, *International Conference on Information Security and Assurance*, Springer Berlin Heidelberg, 2010, pp. 138–148.
- [28] R. Karimi, F. Yousefi, M. Ghaedi, K. Dashtian, Back propagation artificial neural network and central composite design modeling of operational parameter impact for sunset yellow and azur (II) adsorption onto MWCNT and MWCNT-Pd-NPs: isotherm and kinetic study, *Chemom. Intell. Lab. Syst.*, 159 (2016) 127–137.
- [29] Z. Shahryari, A. Mohebbi, A.S. Goharizi, A.A. Forghani, Application of artificial neural networks for formulation and modeling of dye adsorption onto multiwalled carbon nanotubes, *Res. Chem. Intermed.*, 39 (2013) 3595–3609.
- [30] C. Cojocaru, M. Macoveanu, I. Cretescu, Peat-based sorbents for the removal of oil spills from water surface: application of artificial neural network modeling, *Colloids Surf., A*, 384 (2011) 675–684.
- [31] S. Chowdhury, S. Chakraborty, P.D. Saha, Removal of crystal violet from aqueous solution by adsorption onto eggshells: equilibrium, kinetics, thermodynamics and artificial neural network modeling, *Waste Biomass Valorization*, 4 (2013) 655–664.
- [32] M. Saemi, M. Ahmadi, A.Y. Varjani, Design of neural networks using genetic algorithm for the permeability estimation of the reservoir, *J. Pet. Sci. Eng.*, 59 (2007) 97–107.
- [33] P. Lu, S. Chen, Y. Zheng, Artificial intelligence in civil engineering, *Math. Prob. Eng.*, 2012 (2012) Article ID 145974.
- [34] M. Fan, T. Li, J. Hu, R. Cao, X. Wei, X. Shi, W. Ruan, Artificial Neural Network Modeling and Genetic Algorithm Optimization for Cadmium Removal from Aqueous Solutions by Reduced Graphene Oxide-Supported Nanoscale Zero-Valent Iron (nZVI/rGO) Composites, *Materials*, 10 (2017) 1–22.
- [35] A.M. Ghaedi, M. Ghaedi, A.R. Pouranfard, A. Ansari, Z. Avazzadeh, A. Vafaei, I. Tyagi, S. Agarwal, V.K. Gupta, Adsorption of Triamterene on multi-walled and single-walled carbon nanotubes: artificial neural network modeling and genetic algorithm optimization, *J. Mol. Liq.*, 216 (2016) 654–665.
- [36] H. Pfost, V. Headley, *Methods of Determining and Expressing Particle Size, Feed Manufacturing Technology*, 1976, pp. 512–517.
- [37] US Environmental Protection Agency, Fate, Transport, and Transformation Test Guidelines, Adsorption/Desorption (Batch Equilibrium), USEPA, Washington, DC, OPPTS 835.1230, 2008.
- [38] W.J. Weber, C.T. Miller, Modeling the sorption of hydrophobic contaminants by aquifer materials—I. Rates and equilibria, *Water Res.*, 22 (1988) 457–464.
- [39] Y.S. Ho, G. McKay, A comparison of chemisorption kinetic models applied to pollutant removal on various sorbents, *Process Saf. Environ. Prot.*, 76 (1998) 332–340.
- [40] Y.S. Ho, G. McKay, Sorption of dye from aqueous solution by peat, *Chem. Eng. J.*, 70 (1998) 115–124.
- [41] Y.S. Ho, G. McKay, Pseudo-second order model for sorption processes, *Process Biochem.*, 34 (1999) 451–465.
- [42] W.J. Weber, J.C. Morris, Kinetics of adsorption on carbon from solution, *J. Sanit. Eng. Div.*, 89 (1963) 31–60.
- [43] A.E. Ofomaja, Intraparticle diffusion process for lead(II) biosorption onto mansonia wood sawdust, *Bioresour. Technol.*, 101 (2010) 5868–5876.
- [44] C. Sutherland, C. Venkobachar, A diffusion-chemisorption kinetic model for simulating biosorption using forest macrofungus, *Fomes fasciatus*, *Int. Res. J. Plant Sci.*, 1 (2010) 107–117.
- [45] A.P. Mathews, W.J. Weber Jr., Effects of External Mass Transfer and Intraparticle Diffusion on Adsorption Rates in Slurry Reactors, *AIChE Symposium Series*, Vol. 73, 1977, pp. 91–98.
- [46] T. Furusawa, J.M. Smith, Fluid-particle and intraparticle mass transport rates in slurries, *Ind. Eng. Chem. Fundam.*, 12 (1973) 197–203.
- [47] G.E. Boyd, A.W. Adamson, L.S. Meyers, The exchange adsorption of ions from aqueous solutions by organic zeolites II, *J. Am. Chem. Soc.*, 69 (1947) 2836–2848.
- [48] T. Vermeulen, Theory of irreversible and constant-pattern solid diffusion, *Ind. Eng. Chem.*, 45 (1953) 1664–1670.
- [49] C. Lao-Luque, M. Solé, X. Gamisans, C. Valderrama, A.D. Dorado, Characterization of chromium (III) removal from aqueous solutions by an immature coal (leonardite). Toward a better understanding of the phenomena involved, *Clean Technol. Environ. Policy*, 16 (2014) 127–136.
- [50] D.D. Do, *Adsorption Analysis: Equilibria and Kinetics*, Vol 2, Imperial College Press, London, 1998.
- [51] H. Karimi, M. Ghaedi, Application of artificial neural network and genetic algorithm to modeling and optimization of removal of methylene blue using activated carbon, *J. Ind. Eng. Chem.*, 20 (2014) 2471–2476.
- [52] R. Mahajan, G. Kaur, Neural networks using genetic algorithms, *Int. J. Comput. Appl.*, 77 (2013) 6–11.
- [53] M. Bagheri, S.A. Mirbagheri, Z. Bagheri, A.M. Kamarkhani, Modeling and optimization of activated sludge bulking for a real wastewater treatment plant using hybrid artificial neural networks-genetic algorithm approach, *Process Saf. Environ. Prot.*, 95 (2015) 12–25.

- [54] D.L. Mitic-Stojanovic, A. Zarubica, M. Purenovic, D. Bojic, T. Andjelkovic, A.L. Bojic, Biosorptive removal of Pb²⁺, Cd²⁺ and Zn²⁺ ions from water by *Lagenaria vulgaris* shell, *Water SA*, 37 (2011) 303–312.
- [55] K. Fu, Z. Li, Q. Xia, T. Zhong, Change and Improving of Ammonium Exchange Capacity onto Zeolite in Seawater, 2nd International Conference on Environmental Engineering and Applications IPCBEE, Vol. 17, IACSIT Press, Singapore, 2011, pp. 226–231.
- [56] S.J. Lee, J.H. Park, Y.T. Ahn, J.W. Chung, Comparison of heavy metal adsorption by peat moss and peat moss-derived biochar produced under different carbonization conditions, *Water Air Soil Pollut.*, 226 (2015) 2106–2116.
- [57] J.L. Gardea-Torresday, L. Tang, J.M. Salvador, Copper adsorption by esterified and unesterified fractions of sphagnum peat moss and its different humic substances, *J. Hazard. Mater.*, 48 (1996) 191–206.
- [58] B. Subramanyam, A. Das, Linearized and non-linearized isotherm models comparative study on adsorption of aqueous phenol solution in soil, *Int. J. Environ. Sci. Technol.*, 6 (2009) 633–640.
- [59] B.S. Chittoo, C. Sutherland, Adsorption of phosphorus using water treatment sludge, *J. Appl. Sci.*, 14 (2014) 3455–3463.
- [60] B. Das, N.K. Mondal, R. Bhaumik, P. Roy, K.C. Pal, C.R. Das, Removal of copper from aqueous solution using alluvial soil of Indian origin: equilibrium, kinetic and thermodynamic study, *J. Mater. Environ. Sci.*, 4 (2013) 392–408.
- [61] A.G. El-Said, Biosorption of Pb (II) ions from aqueous solutions onto rice husk and its ash, *J. Am. Sci.*, 6 (2010) 143–150.
- [62] C.F. Baes, R.E. Mesmer, *Hydrolysis of Cations*, Wiley, New York, 1976.
- [63] K. Jiang, T.H. Sun, L.N. Sun, H.B. Li, Adsorption characteristics of copper, lead, zinc and cadmium ions by tourmaline, *J. Environ. Sci.*, 18 (2006) 1221–1225.
- [64] H. Cheng, H. Song, F. Cheng, The effect of ion charge-mass ratio on adsorption of heavy metals on magnetotactic bacteria, *Afr. J. Microbiol. Res.*, 6 (2012) 7564–7571.
- [65] S. Schiewer, B. Volesky, Ionic strength and electrostatic effects in biosorption of protons, *Environ. Sci. Technol.*, 31 (1997) 1863–1871.
- [66] S.G. Pouloupoulos, V.J. Inglezakis, *Adsorption, Ion Exchange and Catalysis: Design of Operations and Environmental Applications*, Elsevier, Netherlands, 2006.
- [67] Y.S. Ho, J.C.Y. Ng, G. McKay, Kinetics of pollutant sorption by biosorbents: review, *Sep. Purif. Rev.*, 29 (2000) 189–232.
- [68] Y. Sağ, Y. Aktay, Mass transfer and equilibrium studies for the sorption of chromium ions onto chitin, *Process Biochem.*, 36 (2000) 157–173.
- [69] J. Gao, Q. Zhang, K. Su, R. Chen, Y. Peng, Biosorption of acid yellow 17 from aqueous solution by non-living aerobic granular sludge, *J. Hazard. Mater.*, 174 (2010) 215–225.
- [70] S.S. Gupta, K.G. Bhattacharyya, Kinetics of adsorption of metal ions on inorganic materials: a review, *Adv. Colloid Interface Sci.*, 162 (2011) 39–58.
- [71] J. Wu, H.Q. Yu, Biosorption of 2,4-dichlorophenol from aqueous solution by *Phanerochaete chrysosporium* biomass: isotherms, kinetics and thermodynamics, *J. Hazard. Mater.*, 137 (2006) 498–508.
- [72] Z. Aksu, E. Kabasakal, Batch adsorption of 2,4-dichlorophenoxy-acetic acid (2,4-D) from aqueous solution by granular activated carbon, *Sep. Purif. Technol.*, 35 (2004) 223–240.
- [73] K.K. Choy, D.C. Ko, C.W. Cheung, J.F. Porter, G. McKay, Film and intraparticle mass transfer during the adsorption of metal ions onto bone char, *J. Colloid Interface Sci.*, 271 (2004) 284–295.
- [74] J.C. Crittenden, R.R. Trussell, D.W. Hand, K.J. Howe, G. Tchobanoglous, *MWH's Water Treatment: Principles and Design*, John Wiley & Sons, New Jersey, 2012.
- [75] R.M. Viegas, M. Campinas, H. Costa, M.J. Rosa, How do the HSDM and Boyd's model compare for estimating intraparticle diffusion coefficients in adsorption processes, *Adsorption*, 20 (2014) 737–746.
- [76] M.N. Almasri, J.J. Kaluarachchi, Modular neural networks to predict the nitrate distribution in ground water using the on-ground nitrogen loading and recharge data, *Environ. Modell. Software*, 20 (2005) 851–871.
- [77] K. Yetilmezsoy, Modeling studies for the determination of completely mixed activated sludge reactor volume: steady-state, empirical and ANN applications, *Neural Network World*, 20 (2010) 559–589.
- [78] A. Akkoyunlu, K. Yetilmezsoy, F. Erturk, E. Oztemel, A neural network-based approach for the prediction of urban SO₂ concentrations in the Istanbul metropolitan area, *Int. J. Environ. Pollut.*, 40 (2010) 301–321.
- [79] G. Garson, Interpreting neural-network connection weights, *Artif. Intell. Expert*, 6 (1991) 46–51.